Dynamics of $A + B \rightarrow C$ reaction fronts under radial advection in three dimensions

Alessandro Comolli, A. De Wit, and Fabian Brau*
Université libre de Bruxelles (ULB), Nonlinear Physical Chemistry Unit, CP231, 1050 Brussels, Belgium

(Received 17 September 2019; published 25 November 2019)

The dynamics of $A + B \rightarrow C$ reaction fronts is studied both analytically and numerically in three-dimensional systems when A is injected radially into B at a constant flow rate. The front dynamics is characterized in terms of the temporal evolution of the reaction front position, r_f, of its width, w, of the maximum local production rate, $R^{\max}$, and of the total amount of product generated by the reaction, n_C. We show that r_f, w, and $R^{\max}$ exhibit the same temporal scalings as observed in rectilinear and two-dimensional radial geometries both in the early-time limit controlled by diffusion, and in the longer time reaction-diffusion-advection regime. However, unlike the two-dimensional cases, the three-dimensional problem admits an asymptotic stationary solution for the reactant concentration profiles where n_C grows linearly in time. The timescales at which the transition between the regimes arise, as well as the properties of each regime, are determined in terms of the injection flow rate and reactant initial concentration ratio.

DOI: 10.1103/PhysRevE.100.052213

I. INTRODUCTION

A sound understanding of the dynamics of reaction-diffusion (RD) fronts is crucial for the description of many phenomena. The seminal works by Kolmogorov *et al.* [1] and Fisher [2] led the way to the study of RD fronts in biology [3,4], chemistry [5,6], ecology [7,8], physics [9,10], and nanotechnology [11], to cite a few.

An important subset of RD fronts is represented by $A + B \rightarrow C$ fronts, which arise when two species A and B, initially separated, are put into contact, diffuse, and react to produce a third species C. Depending on the nature of A, B, and C, this general system can describe a large set of problems in, for example, geochemistry [12,13], catalysis [14], particle physics [15], and finance [16]. A fundamental contribution to the understanding of the dynamics of $A + B \rightarrow C$ RD fronts was given by Gálfi and Rácz [17], who provided analytical results for rectilinear fronts, in which the initial contact interface between A and B is planar. By assuming equal diffusion coefficients for the reactants, they showed that in the long-time limit, or equivalently for fast reactions, the reaction front position, x_f, moves proportionally to $t^{1/2}$, the maximum of the production rate, $R^{\max}$, scales as $t^{-2/3}$ while the width, w, of the front grows like $t^{1/6}$. These results were later confirmed experimentally [18,19] and generalized for arbitrary diffusion coefficients [20,21] and in the short-time regime [22–24].

In many natural and engineered systems, the reactant A is injected at a given flow rate in a region initially occupied by the reactant B. For rectilinear fronts, if the velocity field is constant and orthogonal to the front, the results of Gálfi and Rácz remain valid in the comoving frame. If the advection field is not uniform, however, the dynamics of the $A + B \rightarrow C$ reaction fronts is more complex. Such reaction-diffusion-advection (RDA) fronts have been the subject of several studies with application to combustion [25] and groundwater hydrology [26], among others.

Recently, the dynamics of RDA fronts in two dimensions in the presence of radial injection of A into B has been analyzed [27,28]. Such two-dimensional (2D) RDA models are relevant, for example, in studies on infectious disease spreading [29], precipitation patterns obtained under radial injection conditions [30–33], and, more generally, material synthesis in nonequilibrium conditions [34–36]. It was shown that, in the long-time regime, the front position, r_f, the maximum production rate, $R^{\max}$, and the width, w, feature the same long-time scalings as for the rectilinear front, while, unlike the rectilinear case, varying the injection flow rate allows for tuning the coefficients of these scalings and the total amount of product C.

In many systems, however, a pointlike injection of a species A into a bulk of B is performed in three dimensions and a three-dimensional (3D) formulation is thus required, e.g., for precipitation or dissolution reactions in CO_2 sequestration and remediation of water contamination. The RD front dynamics has been studied in 3D spherical geometry in the case where the reactant A is maintained in contact with B at a point source with a given strength during a finite time [37,38]. The existence of a stationary state has been shown in this case. However, it is still unknown how advection and a continuous injection of the reactant A affect the dynamics of $A + B \rightarrow C$ fronts in such 3D geometry.

In this context, we study theoretically in three dimensions the properties of radially symmetric $A + B \rightarrow C$ fronts subjected to a passive injection of A into B at a constant flow rate $\bar{Q}$ where all species have equal diffusion coefficients. We show that, unlike the two-dimensional case, three distinct temporal regimes exist in three dimensions, the last one representing a stationary state. These three regimes are characterized here in detail, and scalings for r_f, $R^{\max}$, w and for the total amount of product, n_C, are obtained in each case.

*fabian.brau@ulb.ac.be

The paper is structured as follows. In Sec. II we present the dimensionless partial differential equations (PDEs) describing the RDA $A + B \to C$ front evolution, and we study analytically and numerically the stationary regime. In Sec. III we study analytically and numerically the preasymptotic reaction front dynamics, by identifying and characterizing the early-time and the transient temporal regimes. In Sec. IV we compute analytically the temporal evolution of the total amount of product generated by the reaction, n_C, in each regime and compare the scalings to the numerical evolution. Finally, Sec. V summarizes the paper.

II. MODEL AND STATIONARY SOLUTION

We consider a 3D system filled by a reactant B with an initial dimensional concentration $\bar{b}_0$ in which a reactant A in concentration $\bar{a}_0$ is injected radially from a point source at a constant flow rate $\bar{Q}$. Note that, throughout this article, dimensional and dimensionless variables are denoted with and without a bar, respectively. Upon contact between the reactants A and B, the irreversible $A + B \to C$ reaction occurs, where C is the product of the reaction. All species undergo advective and diffusive motion. The dynamics of the system is described by the following set of dimensional partial differential equations:

$$\partial_{\bar{t}}\bar{a} + (\bar{\boldsymbol{v}}\cdot\boldsymbol{\nabla})\bar{a} = D_a\nabla^2\bar{a} - k\bar{a}\bar{b}, \tag{1a}$$

$$\partial_{\bar{t}}\bar{b} + (\bar{\boldsymbol{v}}\cdot\boldsymbol{\nabla})\bar{b} = D_b\nabla^2\bar{b} - k\bar{a}\bar{b}, \tag{1b}$$

$$\partial_{\bar{t}}\bar{c} + (\bar{\boldsymbol{v}}\cdot\boldsymbol{\nabla})\bar{c} = D_c\nabla^2\bar{c} + k\bar{a}\bar{b}, \tag{1c}$$

where $\bar{t}$ is time, $\bar{\boldsymbol{v}}$ is the advective velocity, k the kinetic constant, $\bar{a}$, $\bar{b}$, and $\bar{c}$ are the concentrations of A, B, and C, and D_a, D_b, and D_c are their diffusion coefficients. In the following, we will assume that the diffusion coefficient is the same for all species, namely, $D = D_a = D_b = D_c$. The nondimensionalization of the PDEs (1) is carried out by rescaling time by $\tau = 1/k\bar{a}_0$ and space by $\ell = \sqrt{D\tau}$. All concentrations are normalized by the initial concentration $\bar{a}_0$ of the injected reactant such that the initial dimensionless concentration of B is given by

$$\gamma = \bar{b}_0/\bar{a}_0. \tag{2}$$

By assuming flow incompressibility, $\boldsymbol{\nabla}\cdot\bar{\boldsymbol{v}} = 0$, radial symmetry, $\bar{\boldsymbol{v}} = (\bar{v}_r, 0, 0)$, and the flow rate definition, $\bar{Q} = \int_S \bar{\boldsymbol{v}}\cdot\boldsymbol{n}\,dS$ where $\boldsymbol{n} = \boldsymbol{e}_r$ is a unit vector along the radial coordinate, $\bar{r}$, of the spherical system of coordinates centered on the injection point and S is the surface of a sphere of radius $\bar{r}$, the flow field is given by $\bar{v}_r = \bar{Q}/(4\pi\bar{r}^2)$. The dimensionless equations describing the dynamics are then

$$\partial_t a + v_r\partial_r a = \left(\partial_r^2 + 2r^{-1}\partial_r\right)a - ab, \tag{3a}$$

$$\partial_t b + v_r\partial_r b = \left(\partial_r^2 + 2r^{-1}\partial_r\right)b - ab, \tag{3b}$$

$$\partial_t c + v_r\partial_r c = \left(\partial_r^2 + 2r^{-1}\partial_r\right)c + ab, \tag{3c}$$

where t, r, v_r, and Q are the dimensionless time, radial coordinate, velocity field, and flow rate, respectively, with

$$v_r = \frac{Q}{r^2}, \quad \text{where} \quad Q = \frac{\tau}{4\pi\ell^3}\bar{Q} = \frac{\bar{Q}}{4\pi D^{3/2}\tau^{1/2}}. \tag{4}$$

For a relatively fast reaction, such that $\tau = 10^{-3}$ s, a dimensionless flow rate $Q = 100$ corresponds thus to a flow rate $\bar{Q} \simeq 10^{-6}$ ml/s for $D = 10^{-9}$ m^2/s. Similarly, a slower reaction, such that $\tau = 10^3$ s, leads to a flow rate $\bar{Q} \simeq 10^{-3}$ ml/s for the same values of Q and D. Note also that the PDEs (3) are similar to those of the 2D radial case [27,28] except for a factor 2 in the Laplacian operator and for the fact that $v_r \sim r^{-2}$ in three dimensions whereas $v_r \sim r^{-1}$ in two dimensions.

The coupled nonlinear PDEs (3) must be solved with the initial condition $a(r > 0, 0) = c(r, 0) = 0$ and $b(r > 0, 0) = \gamma$ and the boundary conditions $a(r \to 0, t) = 1$, $a(r \to \infty, t) = b(r \to 0, t) = c(r \to 0, t) = c(r \to \infty, t) = 0$ and $b(r \to \infty, t) = \gamma$. For numerical computations, the boundary conditions are applied at $r = r_0 \ll 1$ and $r = r_{\max} \gg 1$ chosen such that the results are insensitive to their values. In general, the coupled PDEs (3) cannot be solved analytically. However, an analytical solution can be obtained in the long-time limit. By subtracting Eq. (3b) from Eq. (3a), we get the following PDE for $u = a - b$:

$$\partial_t u + \left(\frac{Q}{r^2} - \frac{2}{r}\right)\partial_r u - \partial_r^2 u = 0, \tag{5}$$

with the boundary and initial conditions $u(r \to 0, t) = 1$ where $b = 0$ and $a = 1$, $u(r \to \infty, t) = -\gamma$ where $a = 0$, $b = \gamma$, and $u(r, 0) = -\gamma$ for $r > 0$. The quantity u is thus conservative in the sense that it is reaction-independent. The solution of the PDE (5) at finite times must be found numerically. Nevertheless, it admits an analytical stationary solution u_s satisfying the boundary conditions:

$$u_s(r) = 1 - (1 + \gamma)\exp(-Q/r). \tag{6}$$

Here and in the following, the subscript s stands for *stationary*. The existence of a stationary solution means that, unlike the previously studied 2D cases with advection, the 3D RDA spherical reaction front eventually stops beyond a given distance. The location of this stationary sphere is the radial coordinate $r_{\rm fs}$, obtained in the next section, at which the incoming flux $\boldsymbol{j}_a$ of A across the surface of the sphere is exactly compensated by the incoming flux $\boldsymbol{j}_b$ of B. For equal diffusion coefficients, this condition reads $\int_S(\boldsymbol{j}_a - \boldsymbol{j}_b)\cdot d\boldsymbol{S} = \int_V[\boldsymbol{\nabla}\cdot(\boldsymbol{j}_a - \boldsymbol{j}_b)]dV = 0$ where $\boldsymbol{j}_i = -\boldsymbol{\nabla}i + \boldsymbol{v}i$, with $i = a, b$. For radially symmetric fields in spherical coordinates such that $\boldsymbol{j}_i = j_i\boldsymbol{e}_r = (-\partial_r i + v_r i)\boldsymbol{e}_r$, the divergence-free condition reads $j_a - j_b = \alpha/r^2$, where α is a constant. The solution of this equation, with the boundary conditions for $u = a - b$ mentioned above, is $u = u_s$, with u_s given by Eq. (6). The divergence-free condition in rectilinear [17] or 2D radial [27] geometries cannot be satisfied by physical concentration fields. Figure 1 shows how the solution $u(r, t)$ of Eq. (5) converges to the stationary solution (6) and gives the corresponding a_s and b_s concentration profiles in the asymptotic stationary regime. Some properties of the stationary reaction front are derived in the next sections.

A. Reaction front position

The reaction front position, r_f, is defined as the location at which $a = b$ or, equivalently, $u = 0$. As shown below, this location coincides with the distance from the inlet at which the production rate, $R = ab$, is maximum, i.e., where the reaction

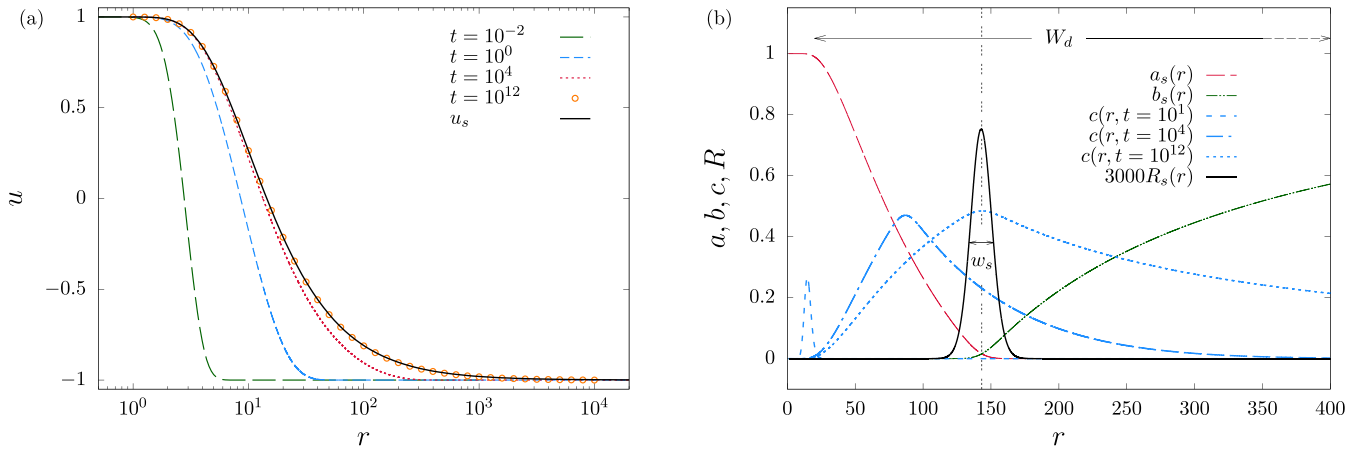

FIG. 1. (a) Numerical radial profile $u(r,t)$ for $Q = 100$, $\gamma = 1$ at different times and analytical stationary solution (6). (b) Numerical stationary concentration profiles a_s and b_s, production rate, $R_s = a_s b_s$, and front width, w_s, for $Q = 100$ and $\gamma = 1$. The evolution of concentration profile of the product C is also shown. The vertical dashed line indicates $r_{\rm fs}$. Numerical solutions are considered stationary for $t > 10^3 t_{\rm TS}$, where $t_{\rm TS}$ is defined as in Eq. (34).

is more intense, when $r_f \gg 1$; see also Ref. [17,27] and Sec. II B. The stationary reaction front position, $r_{\rm fs}$, is obtained by imposing $u_s = 0$ in Eq. (6) and reads

$$r_{\rm fs} = \frac{Q}{\ln(1+\gamma)}, \quad \bar{r}_{\rm fs} = \frac{\bar{Q}}{4\pi D \ln(1+\gamma)}, \tag{7}$$

where $\bar{r}_{\rm fs}$ is the dimensional stationary front position. Notice that these results are valid only for $Q, \gamma \neq 0$. Equation (7) shows that the limit radial distance from the injection source that can be reached by the front increases linearly with the injection flow rate Q and decreases logarithmically as the ratio γ of initial reactant concentrations increases. This is logical as the larger the injection flow rate Q, the further will A be advected before its consumption by the reaction can counterbalance the incoming reactant flux. In the same spirit, the larger γ, the more reactant B is available to consume the injected A and the smaller the radius of the stationary reaction sphere.

B. Production rate

The production rate of the species C is given by

$$R(r,t) = a(r,t)\, b(r,t). \tag{8}$$

The maximum of the production rate, $R^{\max}$, and the local value, R_f, of the production rate evaluated at the front position, r_f, are given by

$$R^{\max}(t) = \max_{0 \leqslant r < \infty} R(r,t), \quad R_f(t) = R(r_f(t), t), \tag{9}$$

In the following, we quantify the impact of Q and γ on the stationary production rate $R_s(r)$ and on its local values $R_{\rm fs}$ and $R_s^{\max}$. To this end, we write Eq. (3a) in terms of the stationary quantities a_s and u_s:

$$d_r^2 a_s + \left(\frac{2}{r} - \frac{Q}{r^2}\right) d_r a_s - a_s(a_s - u_s) = 0. \tag{10}$$

Following Refs. [17,27], we expand the solution $u_s(r)$ around the stationary front position, $r_{\rm fs}$, by assuming that the stationary front width, w_s, defined as the width of the production rate distribution, is much smaller than the depletion zone of a_s and b_s defined as the region of size W_d where the reactant concentrations vary significantly; see Fig. 1(b). Since this zone grows diffusively [17,27], this hypothesis is equivalent to the assumption that the width of the reaction front, w, does not grow faster than $t^{1/2}$ before reaching the stationary state. This hypothesis, which is verified in Sec. III, implies that, at times large enough, the reaction occurs in a region near $r = r_{\rm fs}$ which is small compared to the depletion zone. Therefore, these concentrations can be replaced by their local approximation near $r = r_{\rm fs}$. Since by definition of the front position, $u_s(r_{\rm fs}) = 0$, the expansion of u_s around $r_{\rm fs}$ gives, from Eq. (6):

$$u_s(r) = -K_s\,(r - r_{\rm fs}) + O[(r - r_{\rm fs})^2], \tag{11a}$$

$$K_s = \ln^2(1+\gamma)/Q, \tag{11b}$$

where K_s is simply the first derivative of u_s evaluated at $r = r_{\rm fs}$ given by Eq. (7).

Using Eq. (11), Eq. (10) becomes

$$d_z^2 G(z) + \left[\frac{2}{z + r_{\rm fs}} - \frac{Q}{(z + r_{\rm fs})^2}\right] d_z G(z) - G^2(z) - K_s\, z\, G(z) = 0, \tag{12}$$

where $z = r - r_{\rm fs}$ and $a_s(r) = G(r - r_{\rm fs})$. For such a local analysis, the boundary conditions must be adapted. On the right side of the stationary reaction front ($r > r_{\rm fs}$), the concentration of A is vanishing and $G(z) = 0$ for $z \to \infty$. On the left side of the reaction front ($r < r_{\rm fs}$), the concentration of B is vanishing and $a_s = u_s$. Therefore, $G(z) = u_s(z) = -K_s\, z$ for $z \to -r_{\rm fs} \simeq -\infty$ where we assume that the flow rate is such that $Q \gg \ln(1+\gamma)$, i.e., $r_{\rm fs} \gg 1$. In this limit of large $r_{\rm fs}$, the terms within the square brackets of Eq. (12) can be neglected. In addition, introducing the change of variables

$$G = K_s^{2/3}\, \tilde{G} \quad \text{and} \quad z = K_s^{-1/3}\, \tilde{z}, \tag{13}$$

Eq. (12) reduces to

$$d_{\tilde{z}}^2 \tilde{G}(\tilde{z}) = \tilde{G}^2(\tilde{z}) + \tilde{z}\tilde{G}(\tilde{z}), \tag{14}$$

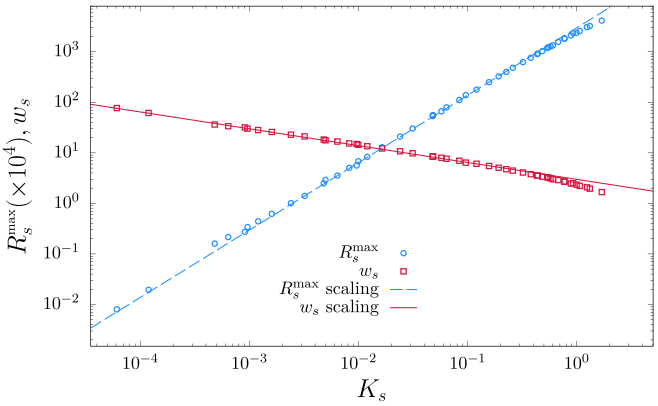

FIG. 2. Stationary maximum production rate, $R_s^{\max}$, and reaction front width, w_s, as a function of K_s obtained through numerical computations for different values of $Q \in [4, 10^3]$ and $\gamma \in [1/40, 20]$. The dashed and solid lines represent the scalings (17) and (20), respectively.

with the boundary conditions $\tilde{G}(\tilde{z}) = -\tilde{z}$ for $\tilde{z} \to -\infty$ and $\tilde{G}(\tilde{z}) = 0$ for $\tilde{z} \to \infty$. This scaling function is thus the same as in rectilinear and 2D radial geometries for $t \gg 1$ [17,27].

Using Eqs. (11a) and (13) together with the definition of z and G, the stationary production rate reads

$$\begin{aligned} R_s(r) &= a_s(r)b_s(r) = a_s(r)[a_s(r) - u_s(r)] \\ &= G(z)[G(z) + Kz] = K_s^{4/3}[\tilde{G}^2(\tilde{z}) + \tilde{z}\tilde{G}(\tilde{z})], \\ &= K_s^{4/3} G(\tilde{z})G(-\tilde{z}) \equiv K_s^{4/3}\tilde{R}_s(\tilde{z}), \end{aligned} \tag{15}$$

where we have used the identity $G(-\tilde{z}) = \tilde{G}(\tilde{z}) + \tilde{z}$ [17]. Indeed, changing the sign of $\tilde{z}$ in Eq. (14) and in its boundary conditions and substituting $G(-\tilde{z})$ by $\tilde{G}(\tilde{z}) + \tilde{z}$ leave Eq. (14) and its boundary conditions unchanged. Consequently, provided $r_{\rm fs}$ is large enough, the reaction rate R is symmetric with respect to its maximum, which is located at $r = r_{\rm fs}$:

$$R_{\rm fs} = R_s^{\max}. \tag{16}$$

Figure 1(b) shows that R is indeed symmetric with respect to its maximum and that the position of its maximum coincides with $r_{\rm fs}$ where $a_s = b_s$. The maximum of the production rate is then simply obtained by setting $\tilde{z} = 0$ ($r = r_{\rm fs}$) in Eq. (15):

$$R_s^{\max} = G(0)^2\, K_s^{4/3} = 0.298\left[\frac{\ln^2(1+\gamma)}{Q}\right]^{4/3}, \tag{17}$$

where we have used the definition of K_s [see Eq. (11b)] and the numerical value of $G(0)$ [17].

Figure 2 shows the evolution of $R_s^{\max}$ as a function of K_s computed from numerical solutions of Eqs. (3) for several values of Q and γ. A good agreement is found with the scaling (17) provided we stay in the regime where this scaling has been obtained, namely, $r_{\rm fs} \gg 1$ or, equivalently, $Q \gg \ln(1+\gamma)$. Since $\gamma \leqslant 20$ in Fig. 2 and $K_s = \ln(1+\gamma)/r_{\rm fs}$, this condition is equivalent to $K_s \ll 1$. The scaling (17) shows that the maximum production rate of C in the stationary reaction sphere, $R_s^{\max}$, can be increased by increasing the ratio of initial concentrations γ or decreasing the flow rate Q at a fixed concentration of reactants.

C. Reaction front width

The width of the reaction front, w, can be defined as the variance of production rate, R. Hence, the width of the stationary reaction front, w_s, reads

$$w_s^2 = \frac{\int_0^\infty dr\,(r - r_{\rm fs})^2 R_s(r)}{\int_0^\infty dr\, R_s(r)}. \tag{18}$$

Applying the change of variable $(r - r_{\rm fs}) = K_s^{-1/3}\,\tilde{z}$ and using Eq. (15), this last relation becomes

$$w_s^2 = K_s^{-2/3}\left[\frac{\int_{-K_s^{1/3} r_{\rm fs}}^\infty d\tilde{z}\,\tilde{z}^2 \tilde{R}_s(\tilde{z})}{\int_{-K_s^{1/3} r_{\rm fs}}^\infty d\tilde{z}\,\tilde{R}_s(\tilde{z})}\right]. \tag{19}$$

To obtain the scaling (17), we have assumed that $r_{\rm fs} \gg 1$ or, equivalently by using Eq. (7), that $\ln(1+\gamma) = \epsilon Q$ with $\epsilon \ll 1$. This implies that $K_s^{1/3} r_{\rm fs} = (Q/\epsilon)^{1/3}$ is much larger than 1 provided Q is of order 1 or larger. Notice that, if γ is very small, i.e., B is initially much less concentrated than A, one can have $r_{\rm fs} \gg 1$ and $K_s^{1/3} r_{\rm fs} \ll 1$ provided Q is also very small. For example, using $\gamma = 10^{-6}$ and $Q = 10^{-4}$, we get $r_{\rm fs} = 10^2$ and $K_s^{1/3} r_{\rm fs} = 10^{-2}$. Dismissing this later possibility, namely assuming that $Q \gg \ln(1+\gamma)$ and $Q^2 \gg \ln(1+\gamma)$, the lower limit of integration in Eq. (19) can be replaced by $-\infty$ since the function $\tilde{R}_s$ is sharply peaked around $\tilde{z} = 0$, i.e., $r = r_{\rm fs}$. Consequently, the factor within the square brackets of Eq. (19) is a constant independent on K_s such that

$$w_s \simeq d\, K_s^{-1/3} = d\left[\frac{Q}{\ln^2(1+\gamma)}\right]^{1/3}. \tag{20}$$

The constant $d \simeq 2$ can be computed numerically using its definition given in Eq. (19) and the definition of $\tilde{R}_s$ given in Eq. (15) once the function G is obtained by solving Eq. (14) [17]. Equation (20) shows that the width of the stationary front increases with Q, i.e., for stronger advection, and is on the contrary narrower when γ increases, i.e., for stronger reaction. Figure 2 shows the good agreement between the width of the stationary reaction front, $w_s(K_s)$, computed from numerical solutions of Eqs. (3) for different values of Q and γ and the scaling (20) provided $K_s \ll 1$, which corresponds to the regime for which the scaling (20) has been derived, and $d = 3.0$. The different constant d simply comes from the fact that w_s is computed as the width at half-height from the numerical solutions of Eqs. (3). The value of the constant is then close to the one obtained for the 2D radial case where the width was also computed in the same way [27].

The main results for the 3D stationary regime, as well as their domain of validity, can be summarized as follow. The stationary reaction front is characterized by its position r_s, Eq. (7), which has been obtained without any assumptions on Q and γ, by its maximum value $R_s^{\max}$, Eq. (17), which is valid provided $Q \gg \ln(1+\gamma)$ and by its width w_s, Eq. (20), which was derived by assuming that $Q \gg \ln(1+\gamma)$ and $Q^2 \gg \ln(1+\gamma)$.

Finally, returning to the dimensional variables, we note that the stationary front position, $\bar{r}_{\rm fs}$, is governed by the flow rate, $\bar{Q}$, the diffusion coefficient, D, and the ratio of the initial concentrations of the reactants, γ, but does not depend on the kinetic constant k [see Eq. (7)]. In contrast, the stationary maximum production rate, $\bar{R}_s^{\max}$, is a function of all these

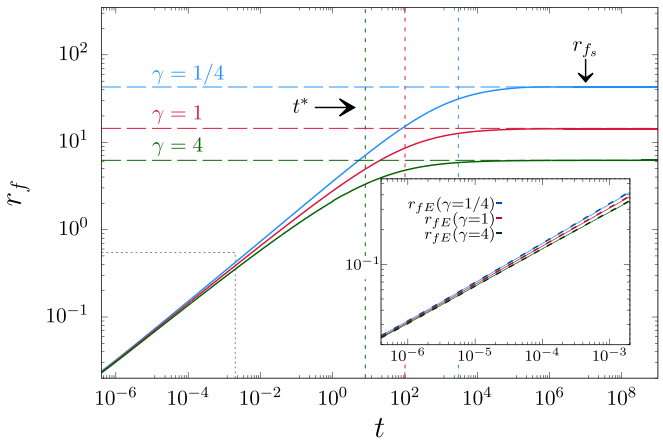

FIG. 3. Temporal evolution of the front position. Solid lines refer to numerical solutions of Eqs. (3) with $Q = 10$ and different values of γ. Horizontal dashed lines are the stationary front positions, $r_{\rm fs}$, given by Eq. (7). Vertical dashed lines show the transition times, t^*, defined by Eq. (23). The inset shows a zoom in the evolution at small time delimited by the dashed rectangle in the main graph.

parameters whereas the stationary width of the front, $\bar{w}_s$, is fixed by $\bar{Q}$, k, and γ but does not depend on the diffusion coefficient.

D. Transition timescale

The time at which the stationary regime is reached can be estimated from the temporal evolution of the front position, $r_f(t)$. Figure 3 shows that, before reaching its stationary value given by Eq. (7), the front position evolves in time according to an early-time behavior $r_{\rm fE}$ approximated as (see the Appendix)

$$r_{\rm fE}(t) = r_f^{\rm ad}(t) + \sqrt{\frac{12}{7}}\,\mathrm{erf}^{-1}\left(\frac{1-\gamma}{1+\gamma}\right)\sqrt{t}, \qquad (21)$$

where the function $\mathrm{erf}(x)$ is the error function [39, p. 159] and $r_f^{\rm ad}$ is the leading term which describes the front movement by advection only according to volume conservation. Neglecting reaction and diffusion, the dimensional volume occupied by the injected reactant is $\bar{V} = \bar{Q}\bar{t} = 4\pi\bar{r}_f^3/3$. Therefore, using (4), we obtain the following dimensionless relation:

$$r_f^{\rm ad}(t) = (3Qt)^{1/3}. \qquad (22)$$

The second term of (21) is a small correction at short time (as long as γ is not extremely large or small) and takes into account the effects due to the reaction. We see that, as in the 2D radial case [27], the front motion is purely due to volume conservation when both reactants have the same initial concentration, $\gamma = 1$. When $\gamma < 1$, i.e., when A is initially more concentrated than B, the second term of Eq. (21) is positive and the front position is then ahead of the position expected from volume conservation, whereas it is a little bit behind it when $\gamma > 1$ since the second term of Eq. (21) is then negative. Note also that the early-time expression of $r_{\rm fE}$, see Eq. (21), involves the sum of two distinct powers of t. This explains why the temporal evolution of the front position for different values of γ does not lead to parallel curves in the log-log plot shown in Fig. 3.

In the 2D radial case, there is no stationary regime and $r_f \sim (Qt)^{1/2}$ at all times; the reaction affects only the coefficient of the power-law growth [27]. In the 3D case, the time, t^*, needed for the temporal evolution of the front position to saturate to its stationary position $r_{\rm fs}$ can be estimated by equating Eq. (22) to $r_{\rm fs}$ given by Eq. (7):

$$t^* = \frac{Q^2}{3\ln^3(1+\gamma)}, \quad \bar{t}^* = \frac{\bar{Q}^2}{3(4\pi)^2 D^3 \ln^3(1+\gamma)}. \qquad (23)$$

As an example, by taking $\gamma = 1$, $D = 10^{-9}$ m^2/s and $\bar{Q} = 0.01$ ml/min, which are typical values used in some laboratory experiments [27,31], the transition time to enter the stationary reaction sphere regime is $\bar{t}^* \simeq 2$ days, and the radius of this sphere would be $\bar{r}_{\rm fs} \simeq 2$ cm. In the case of supercritical CO_2 injection in shallow underground aquifers, typical values of the mass flow rate are of the order of 1 Mt/year [40], which correspond to $\bar{Q} \simeq 10^{-2}$ m^3/s. Hence, the transition time for a 3D problem where CO_2 would be consumed by a simple bimolecular reaction is of the order of $\bar{t}^* = 10^{13}$ years!

In the 2D radial case, the transition time between the early and long-time regimes is controlled by the kinetic constant and can be quite small for fast reactions [27]. This timescale corresponds actually to the transition time $t_{\rm ET}$ between the early-time and transient regimes in three dimensions, which is also controlled by k; see Sec. III C. Studying the long-time regime alone in two dimensions is thus relevant for many practical purposes. However, the timescale at which the stationary regime in three dimensions is reached does not involve the kinetic constant and is instead controlled by the flow rate, the diffusion coefficient and γ, as seen in Eq. (23). Therefore, as seen in the example above, t^*, as well as $t_{\rm TS}$, the transition time between the transient and stationary states introduced in Sec. III C, can be quite large, and the stationary regime could, in practice, never be reached in many systems. Therefore, in the next sections we analyze the early and transient regimes existing before the stationary regime is established.

III. PREASYMPTOTIC DYNAMICS

In this section, we study the dynamics of the RDA fronts before the stationary regime is reached, i.e., for $t \ll t^*$. Figure 4 compares the space-time map of the production rate R for the 2D polar and the 3D spherical systems. In both cases, we observe that the production rate drifts away from the inlet with a decreasing velocity due to volume conservation. In addition, diffusion acts by spreading the production rate plume, so that its maximum decreases while its width increases. In the long-time regime, the front position in three dimensions converges to the stationary position $r_{\rm fs}$, while in two dimensions, $r_f(t)$ scales asymptotically as $t^{1/2}$ [27]. The origin of this different behavior is twofold. On one hand, the radial flow velocity decreases faster in three dimensions ($v_r \sim r^{-2}$) than in two dimensions ($v_r \sim r^{-1}$). On the other hand, in three dimensions the amount of reactant B that consumes the reactant A is proportional to the spherical surface, i.e., to r_f^2, while in two dimensions it is proportional to the perimeter of the circular front, i.e., to r_f. Hence, in three dimensions, the radial expansion of A is slower and its consumption by reaction is larger than in two dimensions.

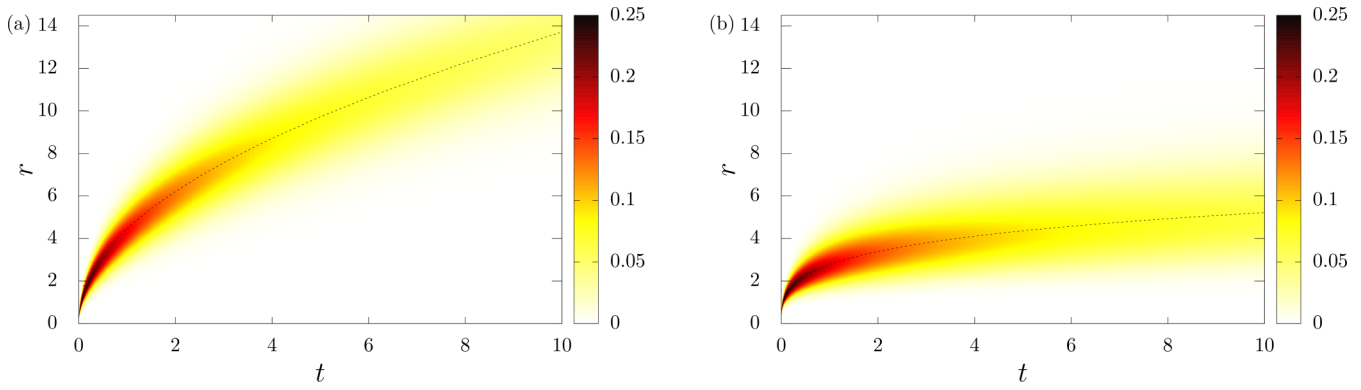

FIG. 4. Space-time maps of the evolution of the production rate $R(r,t)$ for the polar 2D (a) and the spherical 3D systems (b). The dashed line is $r_f(t)$.

In three dimensions, as shown in Fig. 3, the position of the reaction front, r_f, grows as $t^{1/3}$ until it saturates in the stationary regime. On the contrary, Fig. 5 shows that the evolution of $R^{\max}$ and w undergoes two distinct temporal regimes characterized by different power laws before saturating. Namely, we observe (1) an early-time regime characterized by a constant $R^{\max}$ and by a diffusive growth of the front width ($w \sim t^{1/2}$) and (2) a transient regime characterized by a decrease of $R^{\max}$ proportional to $t^{-2/3}$ and by an increase of the front width proportional to $t^{1/6}$. These regimes are discussed in detail in the following sections.

A. The early-time regime

At early times, the amount of mixing of A and B is small and the quantity of C produced is therefore also small. In the Appendix we show that asymptotic solutions, which approximate very well the numerical solutions at short time, can be constructed by taking only diffusion and advection into account. These nonreactive solutions read

$$a(r,t) \underset{t\ll 1}{=} \frac{1}{2}\left[1-\operatorname{erf}\left(\sqrt{\frac{7}{12}}\frac{(r-r_f^{\mathrm{ad}})}{\sqrt{t}}\right)\right], \tag{24a}$$

$$b(r,t) \underset{t\ll 1}{=} \gamma[1-a(r,t)], \tag{24b}$$

where r_f^{ad} is the front position in case of simple nonreactive volume conservation in the presence of advection [see Eq. (22)]. Note that, by definition, the front position is the location where the concentrations of both reactants are equal. Imposing $a=b$, Eqs. (24) leads to the expression (21) of r_{fE}.

1. Production rate

The production rate at early times, denoted R_E where the subscript E stands for "early," is given by

$$R_E(r,t) = a(r,t)\,b(r,t) = \gamma a(r,t)[1-a(r,t)], \tag{25}$$

where a and b are given by Eqs. (24). The value of its maximum, $R_E^{\max}$, can be obtained without knowing the explicit form of $a(r,t)$ from $\partial_r R_E(r,t)|_{r=r^{\max}}=0$, which implies $\partial_r a(r,t)|_{r=r^{\max}}=0$ or $a(r^{\max},t)=1/2$. Since a has no extremum for a finite value of r, the maximum production rate, located where $a(r^{\max},t)=1/2$, is readily obtained by substituting $a=1/2$ in Eq. (25). This leads to

$$R_E^{\max} = \gamma/4. \tag{26}$$

The maximum production rate is thus constant for $t \ll 1$ and the larger γ, the larger $R_E^{\max}$ which is logical as more B is then available for the reaction for a fixed concentration of

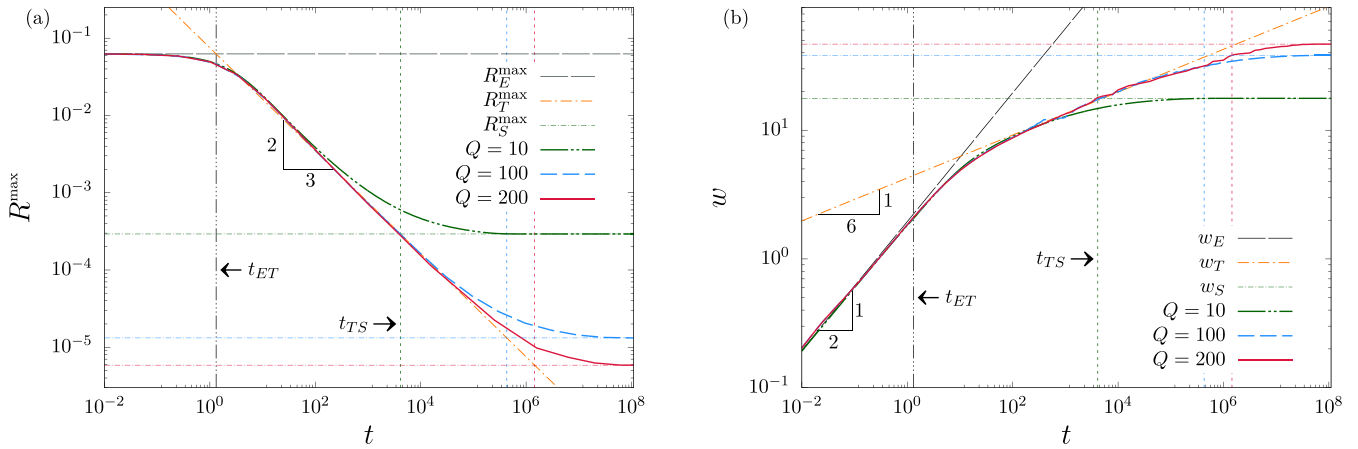

FIG. 5. Temporal evolution of the maximum production rate (a) and of the reaction front width (b) obtained by solving numerically Eqs. (3) with $\gamma = 1/4$. The power laws characterizing the early-time and transient regimes are shown. The vertical dashed-dotted lines indicate the timescale, t_{ET}, at which the transition between the early-time and the transient regimes occurs; see Eq. (33). The vertical dashed lines indicate the timescale, t_{TS}, at which the transition between the transient and the stationary regimes occurs; see Eq. (34).

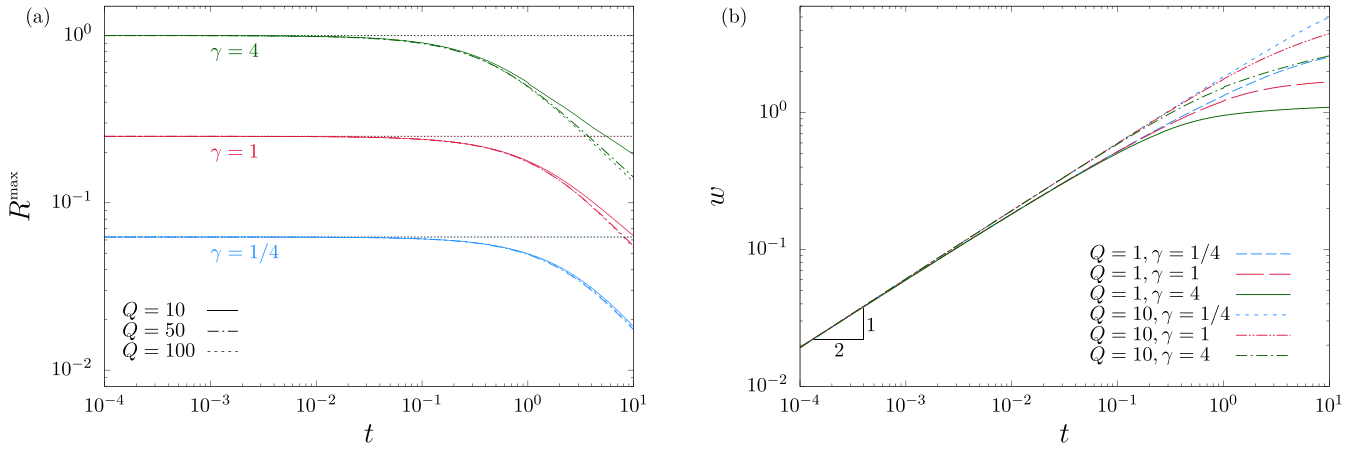

FIG. 6. Early-time behavior of the maximum production rate (a) and the reaction front width (b). The horizontal dotted lines in panel (a) represent the analytical early-time behavior (26).

A. Remarkably, this is the same behavior as for rectilinear [23,24] and 2D radial [28] RD fronts. Actually, this result should be quite general since it does not depend on the particular form of a. Indeed, at times short enough, the reaction term is negligible, and the two equations for A and B decouple and are identical. This implies that, if a is a solution of the advection-diffusion equation with the boundary conditions $a(r \to 0, t) = 1$ and $a(r \to \infty, t) = 0$, then $b = \gamma(1 - a)$ is also a solution with the correct boundary conditions, namely, $b(r \to 0, t) = 0$ and $b(r \to \infty, t) = \gamma$. Therefore, Eq. (25) should be valid at times short enough whatever the geometry, which leads directly to Eq. (26). Figure 6(a) shows the good agreement, up to a dimensionless time of order 1, between the early-time scaling (26) and the early-time evolution of the maximum production rate obtained from numerical solutions of Eqs. (3).

Finally, we can compute the position of the maximum production rate at early times. As shown above, it is solution of the equation $a(r^{\max}, t) = 1/2$. Using the expression (24a) for a, this equation becomes $\mathrm{erf}[\sqrt{7}(r^{\max} - r_f^{\mathrm{ad}})/\sqrt{12t}] = 0$, the unique solution of which is

$$r^{\max}(t) = r_f^{\mathrm{ad}}(t). \tag{27}$$

2. *Reaction front width*

The asymptotic expressions of a and b valid at short times [see Eq. (24)] show clearly that their width scales as $w \sim t^{1/2}$. It can be confirmed by computing the width as the variance of production rate, R:

$$w^2(t) = \frac{\int_0^\infty dr\,[r - r^{\max}(t)]^2 R(r,t)}{\int_0^\infty dr\,R(r,t)}, \tag{28}$$

where $r^{\max} = r_f^{\mathrm{ad}}$ is the radial position of the maximum of the production rate [see Eq. (27)]. By applying the change of variable $z = (r - r_f^{\mathrm{ad}})/\sqrt{t}$ in Eq. (28), and using Eq. (25) of the production rate, the early-time reaction front width w_E reads

$$w_E^2(t) = t\,\frac{\int_{-r_f^{\mathrm{ad}}/\sqrt{t}}^\infty dz\,z^2\,a(z)[1 - a(z)]}{\int_{-r_f^{\mathrm{ad}}/\sqrt{t}}^\infty dz\,a(z)[1 - a(z)]}, \tag{29}$$

where $2a(z) = 1 - \mathrm{erf}(\sqrt{7/12}\,z)$ [see Eq. (24a)]. In the limit $t \to 0$, the lower limits of integration tend to $-\infty$ since $r_f^{\mathrm{ad}} \sim t^{1/3}$ [see Eq. (22)]. The remaining integrals can then be computed exactly, which leads to

$$w_E(t) = (5/7)^{1/2}\,t^{1/2} \simeq 0.85\,t^{1/2}. \tag{30}$$

The short-time behavior $w_E(t) = 1.95\,t^{1/2}$, obtained by solving numerically Eqs. (3) for several values of Q and γ, is shown in Figs. 5(b) and 6(b) and confirms that the width of the reaction front grows as $t^{1/2}$, which is a simple consequence of diffusion. The short-time analysis performed in this section predicts also that w_E is independent on γ and Q; see Fig. 6(b). Notice however that, as mentioned in Sec. II C, the reaction front width has been computed numerically as the width at half the maximum of the production rate curve, rather than from its variance. We show in the Appendix that a factor 1.95 instead of 0.85 is obtained for the short-time scaling of w_E when the width is computed as the width at half-height.

B. The transient regime

Figure 5 shows that a transient regime exists before the system reaches a stationary state. In this regime, numerical results suggest that the maximum production rate and the width scale as

$$r_{\mathrm{fT}}(t) = r_f^{\mathrm{ad}}(t) + c_r(\gamma)\,t^{1/2}, \tag{31a}$$

$$R_T^{\max}(t) = G(0)^2\,K_T^{4/3}\,t^{-2/3} \equiv c_R(\gamma)\,t^{-2/3}, \tag{31b}$$

$$w_T(t) = 2.89\,K_T^{-1/3}\,t^{1/6} \equiv c_w(\gamma)\,t^{1/6}, \tag{31c}$$

where $G(0)^2$ is given in Eq. (17), $c_r \approx \sqrt{12/7}\mathrm{erf}^{-1}[(1 - \gamma)/(1 + \gamma)]$ is the coefficient of the early-time second-order term in Eq. (21), and the subscript T stands for "transient." Notice that a better fit of c_r obtained through numerical computations and shown in Fig. 7(a) would be obtained by substituting $\gamma \to 5\gamma/4$. Remarkably, the temporal evolutions (31) are the same as those obtained in the long-time limit for rectilinear and 2D radial geometries [17,27]. However, the specific values of the factors depend on the geometry. When Q is large enough, such that the transient regime exists [see

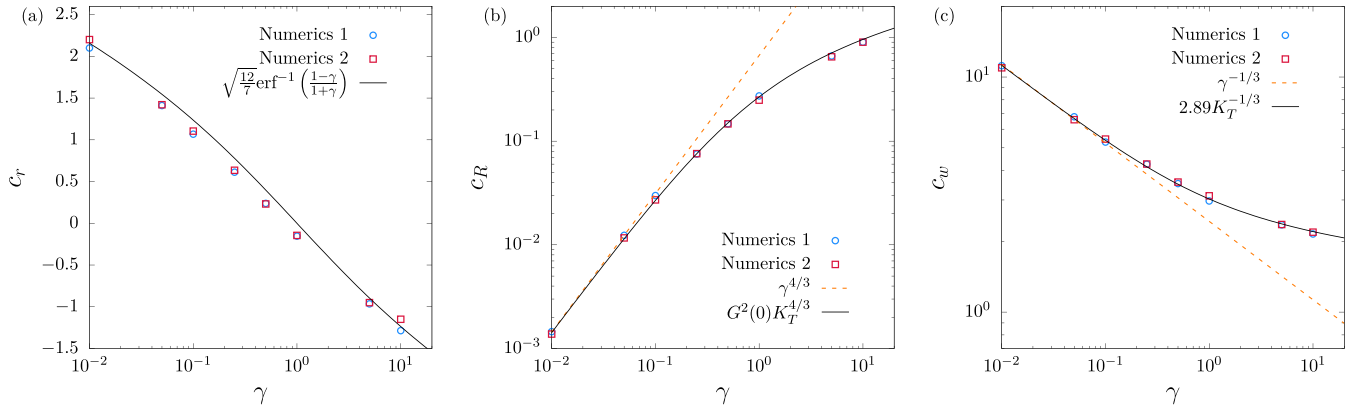

FIG. 7. Evolution of the coefficients c_r (a), c_R (b), and c_w (c) defined by Eqs. (31a), (31b), and (31c) as a function of γ. The following values of Q were used. For the first numerical dataset (blue circles), $Q = 5$ for $\gamma < 0.1$, $Q = 100$ for $\gamma \in [0.1, 1]$, $Q = 200$ for $\gamma = 5$, and $Q = 300$ for $\gamma = 10$. For the second numerical dataset (red squares), $Q = 10$ for $\gamma = 0.01$, $Q = 300$ for $\gamma = 0.05$, $Q = 200$ for $\gamma \in [0.1, 1]$, $Q = 300$ for $\gamma = 5$, and $Q = 400$ for $\gamma = 10$.

Eq. (35)], the coefficient K_T depends only on γ. This behavior of K_T is reminiscent of the one observed for the corresponding coefficient K in the long-time limit of a 2D radial system, which depends also only on γ when Q is large enough (see Fig. 2 in Ref. [27]). The scaling laws (31b) and (31c) also show that the factors involve the same function K_T to the power $4/3$ and $-1/3$ for $R_T^{\max}$ and w_T, respectively. This is exactly the same as for the long-time regime in rectilinear and 2D radial systems. The same structure is also obtained for the stationary solutions $R_s^{\max}$ and w_s; see Eqs. (17) and (20).

Returning to the dimensional variables, we note that the front position, $\bar{r}_{\mathrm{fT}}$, is the sum of an advective term, $\bar{r}_f^{\mathrm{ad}}$, and a term evolving diffusively in time the sign of which is determined by the value of γ; see Fig. 7. Therefore, the temporal evolution of $\bar{r}_{\mathrm{fT}}$ is governed by the flow rate $\bar{Q}$, the diffusion coefficient, D, and the ratio of the initial concentrations of the reactants, γ, but does not depend on the kinetic constant k. In contrast, the temporal evolution of the width of the front, $\bar{w}_T$, involves D, k, and γ but does not depend on the flow rate, whereas the temporal evolution of the maximum production rate, $\bar{R}_T^{\max}$, depends only on k and γ and is thus governed solely by the reaction.

We did not obtain the expression of K_T analytically. Instead, we have fitted with power laws the numerical evolution of $R_T^{\max}$ and of w_T as a function of time in the transient regime to extract the expressions of c_R and c_w. As shown in Fig. 7, a good agreement is obtained provided

$$K_T(\gamma) = 0.736\,\ln(1 + 5\gamma/2). \tag{32}$$

Therefore, at a given time t, when γ increases the maximum of the production rate logically increases, whereas the reaction front has a smaller width.

Notice that, in the transient regime, the front position r_f is still essentially equal to $r_f^{\mathrm{ad}}(t)$, up to a small correction scaling as $t^{1/2}$, which vanishes when $\gamma = 1$, as in the early-time regime; see also Fig. 3. This behavior is also reminiscent of the one observed for the rectilinear and 2D radial cases where r_f grows as $t^{1/2}$ at all times. In the 3D case, the scaling of r_f is affected only when the system approaches the stationary regime.

C. Transition timescales

The characteristic timescales at which the transient regime starts and ends can be computed using the scalings of $R^{\max}$ in the various regimes. The timescale, t_{ET}, at which the transition between the short-time and the transient regimes occurs can be determined by equating the early-time expression (26) of $R_E^{\max}$ and its expression (31b) in the transient regime and using Eq. (32):

$$t_{\mathrm{ET}}(\gamma) \simeq 0.7\,\frac{\ln^2(1 + 5\gamma/2)}{\gamma^{3/2}}, \quad \bar{t}_{\mathrm{ET}} = \frac{t_{\mathrm{ET}}}{k\bar{a}_0}, \tag{33}$$

where $\bar{t}_{\mathrm{ET}}$ is the dimensional transition time between the early-time and the transient regime. The time at which this transition occurs is thus independent on the flow rate as shown in Fig. 5. The timescale t_{ET} is a nonmonotonic function of γ which grows as $\gamma^{1/2}$ when $\gamma \ll 1$ and decreases as $\ln^2(5\gamma/2)/\gamma^{3/2}$ when $\gamma \gg 1$. Therefore, it reaches a maximum value equal to 1.34 when $\gamma \simeq 1/3$.

Analogously, the timescale, t_{TS}, at which the transition between the transient and the stationary regimes occurs can be determined by equating the corresponding expressions of $R^{\max}$, given by Eqs. (17) and (31b), and using Eq. (32):

$$t_{\mathrm{TS}}(Q, \gamma) \simeq \frac{Q^2}{2}\,\frac{\ln^2\left(1 + \frac{5\gamma}{2}\right)}{\ln^4(1 + \gamma)}, \quad \bar{t}_{\mathrm{TS}} = \frac{t_{\mathrm{TS}}(\bar{Q}, \gamma)}{(4\pi)^2 D^3}, \tag{34}$$

where $\bar{t}_{\mathrm{TS}}$ is the dimensional transition time between the transient and the stationary regime. The time at which this transition occurs depends thus on the flow rate as shown in Fig. 5. The quantity t_{TS}/Q^2 is a monotonically decreasing function of γ which varies as γ^{-2} when $\gamma \ll 1$ and as $\ln^2(5\gamma/2)/\ln^4(\gamma)$ when $\gamma \gg 1$. Therefore, t_{TS} diverges when $\gamma \to 0$ since the stationary regime can be reached only if there is a reaction to consume the injected species.

Notice that the transient regime is noticeable only when the power-law behavior has enough time to develop. Numerical evidence suggests that this condition is satisfied when the ratio $\sigma^2 = t_{\mathrm{TS}}/t_{\mathrm{ET}}$ is such that $\sigma > \sigma_{\min} \simeq 47$. By using Eqs. (33) and (34), we obtain the following constraint on the injection

flow rate for the existence of a transient regime:

$$Q > Q_{\min}(\gamma) \simeq 1.2\,\sigma_{\min}\frac{\ln^2(1+\gamma)}{\gamma^{3/4}}. \tag{35}$$

The quantity $Q_{\min}/\sigma_{\min}$ is a nonmonotonic function of γ which grows as $\gamma^{5/4}$ when $\gamma \ll 1$ and decreases as $\ln^2(\gamma)/\gamma^{3/4}$ when $\gamma \gg 1$. It reaches its maximal value equal to 1.23 when $\gamma \simeq 10.4$. Consequently, a sufficient condition for the existence of a transient regime for any γ is $Q > 3\sigma_{\min}/2 \simeq 70$. If the condition (35) for the injection flow rate Q is not verified, such that the transient regime is not observed, the system evolves directly from the short-time regime to the stationary regime. The timescale for this transition can be estimated by t^* defined by (23). The timescales $t_{\rm TS}$ and t^* arise from two different definitions, which are based on the scalings of $R^{\max}$ and r_f, respectively. Notice that for both choices the transition time is proportional to Q^2, but $t_{\rm TS}$ and t^* differ in their dependence on γ. The discrepancy is traced back to the fact that t^* is defined using the early-time purely advective front position $r_f^{\rm ad}$. Hence, when the transient time regime is fully developed, the adoption of $t_{\rm TS}$ should be preferred since it should be more accurate.

IV. TOTAL AMOUNT OF PRODUCT

We conclude our analysis by studying the temporal evolution of the total amount of product $n_C = \int d\mathbf{r}\, c(\mathbf{r}, t)$ generated by the reaction. Because of radial symmetry, it reduces to

$$n_C(t) = 4\pi \int_0^\infty dr\, r^2 c(r, t). \tag{36}$$

To compute the integral of the concentration profile of the product C, we multiply Eq. (3c) by $4\pi r^2$ and integrate over the radial coordinate. By recalling that the concentration c and its gradient vanish at the domain boundaries, we find that the terms related to the transport processes are equal to zero as advection and diffusion do not produce any C. Therefore, we simply obtain the following differential equation for n_C:

$$\frac{dn_C(t)}{dt} = 4\pi \int_0^\infty dr\, r^2 R(r, t). \tag{37}$$

Numerical evidence, as well as the analytical asymptotic solutions at early times [see Eq. (24)], show that R is a peaked function around $r = r_f$; see also Fig. 1(b). Therefore, we write the production rate as $R(r, t) = R^{\max}(t)\phi([r - r_f(t)]/w(t))$, where $\phi(z)$ is peaked around $z = 0$ such that $\phi(0) = 1$ and $\phi'(0) = 0$ where the prime is a derivative with respect to the argument. By substituting this expression into Eq. (37) and performing the change of variable $z = (r - r_f)/w$, we obtain

$$\frac{dn_C(t)}{dt} = 4\pi R^{\max} w \int_{-\frac{r_f}{w}}^\infty dz (r_f + zw)^2 \phi(z). \tag{38}$$

From the scalings presented in the previous sections, we have $r_f/w \gg 1$ in all regimes. Indeed, at early times, we have $r_f/w \sim t^{-1/6} \gg 1$ if $t \ll 1$. In the transient regime, we have $r_f/w \sim t^{1/6} \gg 1$ if $t \gg 1$, i.e., if the transient regime extends up to relatively large times. This happens if $t_{\rm TS} \gg 1$ [see Eq. (34)]. This last condition certainly holds since it is less restrictive than the condition $Q \gg \ln(1 + \gamma)$, which was already assumed in Sec. II B. Finally, in the stationary regime, $r_f/w \sim [Q^2/\ln(1 + \gamma)]^{1/3} \gg 1$ if $Q^2 \gg \ln(1 + \gamma)$ as already assumed in Sec. II C. Therefore, we can replace the lower limit of integration in Eq. (38) by $-\infty$ since the function $\phi(z)$ vanishes quickly when $|z| > 0$ and get

$$\frac{dn_C(t)}{dt} = 4\pi R^{\max} w\big[\mu_0 r_f^2 + 2\mu_1 w r_f + \mu_2 w^2\big], \tag{39}$$

where $\mu_n = \int_{-\infty}^\infty dz\, z^n \phi(z)$.

For each temporal regime described in the previous sections, we substitute the temporal scalings of r_f, $R^{\max}$, and w into Eq. (39) to obtain the temporal evolution of the total amount of product n_C after performing the remaining time integration.

Early-time regime. We substitute the early-time relations (22), (26), and (30) into Eq. (39). By taking the leading order for $t \ll 1$, and by performing the time integration, we find that the early-time amount of product $n_{\rm CE}$ scales as

$$n_{\rm CE}(t) = 6.0\mu_0\,\gamma\, Q^{2/3}\, t^{13/6}. \tag{40}$$

Alternatively, we can compute $n_{\rm CE}$ by using the early-time expression (25) of the production rate in Eq. (37) such that the scaling does no longer contain an undetermined factor. Using again the change of variable $z = (r - r_f^{\rm ad})/\sqrt{t}$, we obtain the following expression at the leading order for $t \ll 1$:

$$n_{\rm CE}(t) = \xi\,\gamma\, Q^{2/3}\, t^{13/6}, \tag{41}$$

where $\xi = (72/13)\,3^{1/6}\sqrt{2\pi/7} \simeq 6.3$. We see that the total amount of product increases relatively fast at short times with a power slightly larger than 2. At a given time, it is proportional to the concentration ratio and grows as the flow rate increases.

Transient regime. We use now the transient regime relations (22), (31), and (32) into Eq. (39), and we obtain in the leading order for $t \gg 1$

$$n_{\rm CT}(t) = 14.2\mu_0\, \ln(1 + 5\gamma/2)\, Q^{2/3}\, t^{7/6}. \tag{42}$$

The total amount of product increases thus in time with a power slightly larger than 1. At a given time, it still depends on the concentration ratio, but now logarithmically, and grows as the flow rate increases with the same power as at early times.

Stationary regime. Finally, for the stationary regime, we substitute Eqs. (7), (17), and (20) into Eq. (39) and use the condition $Q^2 \gg \ln(1 + \gamma)$ to obtain, after time integration, the following relation:

$$n_{\rm Cs}(t) = 11.2\mu_0\, Q\, t. \tag{43}$$

Although the reaction front is stationary, the amount of product increases asymptotically linearly with time as a result of the continuous injection of the reactant A. As soon as the injected reactant reaches the steady front position, $r_{\rm fs}$, it is immediately consumed by the reaction with B, so that the front does not move. The product C is then transported by advection and diffusion according to Eq. (3c). Notice that here the temporal evolution (43) of the total amount of product differs from the scaling $n_C \sim t^{1/2}$ observed for RD fronts in rectilinear geometry [17]. In contrast, n_C grows linearly in time as for the 2D radial RDA case [27]. Unlike the 2D radial case, however, the asymptotic behavior does not depend on γ, but only on the flow rate Q through a linear relationship, in contrast

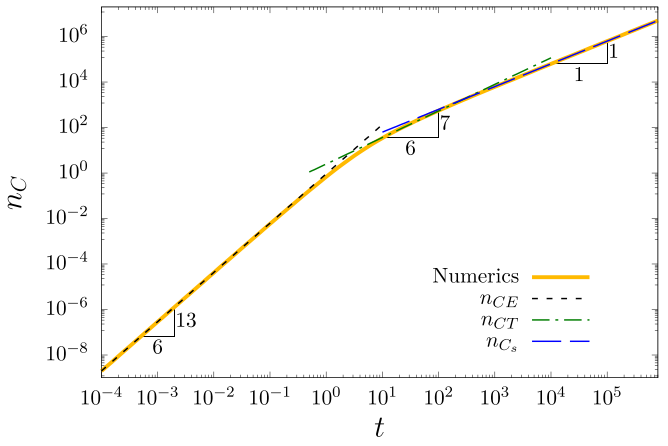

FIG. 8. Temporal evolution of n_C computed using Eq. (37) and R obtained by solving numerically Eqs. (3) with $Q = 5$ and $\gamma = 1/20$. The scalings (41) valid at early times, (42) for the transient regime, and (43) for the stationary regime are also shown.

with the $Q^{1/2}$ dependence of the 2D case. The dimensional form of Eq. (43) reads $\bar{n}_{cs} = 0.9\mu_0 \bar{a}_0 \bar{V}$ which implies that, in the stationary regime, the number of moles of the product C produced by the reaction is proportional to the number of moles of the injected reactant A whatever the concentration of B.

These various scalings describe well the temporal evolution of n_C obtained through numerical computations in their respective regime, as shown in Fig. 8 for $Q = 5$ and $\gamma = 1/20$, provided $\mu_0 \simeq 0.5$ in the transient regime and $\mu_0 \simeq 0.1$ in the stationary regime. Note that the scaling function ϕ, and thus μ_0, is not necessarily the same in each regime. Note also that the scaling (41) is shown in Fig. 8 for the early-time regime and there is thus no fitting parameter in this case.

V. CONCLUSIONS

The characteristics of $A + B \to C$ fronts have been computed in three dimensions when the reactant A is injected radially into B at a constant flow rate. We have shown the existence of three regimes characterized by different scalings for the temporal evolution of the front position, the maximum of the production rate and its width, and of the total amount of product generated. The 3D radial situation differs from the 2D rectilinear and radial cases by the existence of a stationary regime in the long times. We have characterized the stationary front solution in terms of analytical expressions for the front position $r_{\rm fs}$, Eq. (7), the maximum production rate $R_s^{\rm max}$, Eq. (17), the front width w_s, Eq. (20), and the total amount of product $n_{\rm Cs}$, Eq. (43). Like in the two-dimensional radial case, the production rate can be tuned in three dimensions by varying the flow rate Q, as showed by the scaling form (17) derived analytically, $R_s^{\rm max} \sim Q^{-4/3}$, and confirmed by numerical computations. We find that increasing the flow rate Q and/or decreasing the ratio γ of initial concentrations of the reactants increases both the radius $r_{\rm fs}$ and the width w_s, and decreases the maximum production rate $R_s^{\rm max}$ in the stationary reaction sphere. The total amount of product, $n_{\rm Cs}$, increases linearly in time in the stationary regime and, at a given time, increases linearly with Q.

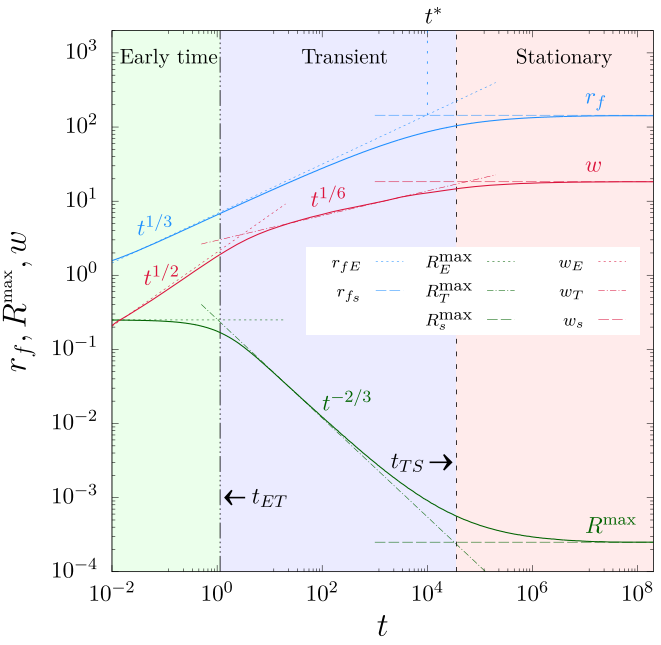

FIG. 9. Summary of the temporal scalings of r_f, w, and $R^{\rm max}$ for $Q = 100$ and $\gamma = 1$.

Before the convergence towards that stationary state, two distinct temporal regimes can be identified from the analysis of the RDA front dynamics: (1) an early-time regime, when the dynamics is dominated by advection and diffusion, and (2) a transient regime, when the dynamics is ruled by the interplay between advection, diffusion, and reaction. The temporal scalings that characterize the RDA front dynamics in the various regimes are summarized in Fig. 9.

At early times, the front position, $r_{\rm fE}$, grows essentially as $r_{\rm fE} \sim t^{1/3}$ [Eqs. (21) and (22)]. This regime is characterized by a constant value of the maximum production rate $R_E^{\rm max} = \gamma/4$ [Eq. (26)], which is fully determined by the ratio γ of the initial concentrations of the reactants, while the front width increases as $w_E \sim t^{1/2}$ [Eq. (30)]. The total amount of product grows as $n_{\rm CE} \sim t^{13/6}$ and, at a given time, varies linearly with γ and increases as $Q^{2/3}$.

The transient regime is only observed in three dimensions when the system has enough time to pass from the early-time to the stationary regime, i.e., only for Q large enough or γ small enough. Here the dynamics is still characterized by $r_{\rm fT} \sim t^{1/3}$ while $R_T^{\rm max} \sim t^{-2/3}$ and $w_T \sim t^{1/6}$ like in the asymptotic long-time limit of the rectilinear [17] and 2D radial case [27]. In this regime, the total amount of product grows as $n_{\rm CT} \sim t^{7/6}$ and, at a given time, varies logarithmically with γ and increases as $Q^{2/3}$. Table I summarizes the results presented in this paper, which are compared with the known results for RD fronts in rectilinear geometry and for RDA fronts in 2D radial geometry.

Unlike its two-dimensional analog, the dynamics of $A + B \to C$ fronts in three dimensions with radial injection admits a stationary solution that has been characterized analytically. The existence of a stationary regime means that the reaction front expands up to a maximum radial distance $r_{\rm fs}$, at which the incoming flux of A across the surface of the sphere of radius $r_{\rm fs}$ is exactly compensated by the incoming flux of B.

TABLE I. Comparison between the temporal scalings of r_f, $R^{\max}$, w, and n_C in different time regimes derived in this work and those, up to constant factors, obtained for a RD rectilinear front and a RDA radial 2D front when both reactants A and B have the same diffusion coefficient, $D_a = D_b$. The number in brackets give the reference to the articles where those scalings have been derived, whereas those in parentheses refer to the related equations of the present article. The scalings for the 2D radial case are those valid at large flow rates ($Q \gg 1$), whereas those in the 3D case are valid if $Q \gg \ln(1+\gamma)$ and $Q^2 \gg \ln(1+\gamma)$. The notations introduced in Ref. [41] are used for the coefficients of the long-time scalings in the rectilinear and radial 2D cases. In rectilinear geometry, if advection at constant velocity is considered, those results are still valid in a frame moving at that speed. In the radial 2D case, the total amount of product at early times can be obtained by integrating the production rate over space, similarly to the computation performed in Sec. IV but in cylindrical coordinate, such that, at large flow rate, we obtain $d_t n_C \sim R^{\max}\, \omega\, r_f \sim \gamma\, Q^{1/2}\, t$. Notice that, depending on the parameters, the long-time regime may not appear in the spherical RDA front case.

		RD rectilinear	2D radial	3D spherical
r_f	Early-time	const $\to t^{3/2}$ [22–24]	$(Qt)^{1/2}$ [28]	$(Qt)^{1/3}$ (22)
	Long-time	$\alpha(\gamma)\, t^{1/2}$ [17]	$(Qt)^{1/2}$ [27,41]	$(Qt)^{1/3}$ (31a)
	Stationary	No	No	$Q/\ln(1+\gamma)$ (7)
$R^{\max}$	Early-time	$\gamma/4$ [22,24]	$\gamma/4$ [28]	$\gamma/4$ (26)
	Long-time	$K_{\rm lin}(\gamma)^{4/3}\, t^{-2/3}$ [17]	$K_{\rm lin}(\gamma)^{4/3}\, t^{-2/3}$ [27,41]	$K_T(\gamma)^{4/3}\, t^{-2/3}$ (31b)
	Stationary	No	No	$K_s(Q,\gamma)^{4/3}$ (17)
w	Early-time	$t^{1/2}$ [22,24]	$t^{1/2}$ [28]	$t^{1/2}$ (30)
	Long-time	$K_{\rm lin}(\gamma)^{-1/3}\, t^{1/6}$ [17]	$K_{\rm lin}(\gamma)^{-1/3}\, t^{1/6}$ [27,41]	$K_T(\gamma)^{-1/3}\, t^{1/6}$ (31c)
	Stationary	No	No	$K_s(Q,\gamma)^{-1/3}$ (20)
n_C	Early-time	$\gamma\, t^{3/2}$ [22]	$\gamma\, Q^{1/2}\, t^2$	$\gamma\, Q^{2/3}\, t^{13/6}$ (40)
	Long-time	$\sigma(\gamma)\, t^{1/2}$ [17]	$j(\gamma)\, Q^{1/2}\, t$ [27,41]	$\ln(1+\frac{5\gamma}{2})\, Q^{2/3}\, t^{7/6}$ (42)
	Stationary	No	No	Qt (43)

These results shed new light on the dynamics of $A + B \to C$ RDA fronts, which can open new investigation branches and be applied in several research fields, according to the nature of A, B and C, which is here left unspecified for sake of generality.

ACKNOWLEDGMENT

The authors acknowledge support by F.R.S.-FNRS under the M-ERA.NET Grant No. R.50.12.17.F.

APPENDIX: EARLY-TIME REGIME

At early times, the amount of mixing of A and B is small and the amount of C produced is also necessarily small. The dynamics is mainly driven by diffusion and also advection since, in this regime, the front moves according to volume conservation. Consequently, we assume that $a(r,t) = a([r - r_f^{\rm ad}(t)]/t^\alpha)$ and $b(r,t) = b([r - r_f^{\rm ad}(t)]/t^\alpha)$, where $\alpha \geqslant 0$ is an arbitrary exponent to be determined and $r_f^{\rm ad}(t) = (3Qt)^{1/3}$ [see Eq. (22)]. Clearly these forms take into account advection and it is expected that $\alpha = 1/2$ due to diffusion. By substituting these ansatz into Eqs. (3), we obtain

$$\frac{d^2a}{dz^2} + \left[\alpha z t^{2\alpha-1} + \frac{2t^\alpha}{r_f^{\rm ad} + zt^\alpha} + \frac{Qt^\alpha}{\left(r_f^{\rm ad}\right)^2} - \frac{Qt^\alpha}{\left(r_f^{\rm ad} + zt^\alpha\right)^2}\right]\frac{da}{dz} - t^{2\alpha}\, ab = 0, \tag{A1}$$

where $z = (r - r_f^{\rm ad})/t^\alpha$. We write here only the equation for a because the one for b is similar. We now consider the scaling limit $t \to 0$ and z fixed, similarly to the long-time analysis where $t \to \infty$ and z fixed [17,27]. In this limit, if $\alpha < 1/2$, the first term inside the square brackets in Eq. (A1) diverges and leads to a nonphysical solution since $d_z a$ cannot vanish everywhere. If $\alpha \geqslant 1/2$, the terms between the square brackets in Eq. (A1) simplify when $t \to 0$ since $r_f^{\rm ad} \sim t^{1/3}$ such that $r_f^{\rm ad} \gg zt^\alpha$. Expanding the second and fourth terms between the square brackets to the leading order, we obtain

$$\frac{d^2a}{dz^2} + \left[\left(\frac{2}{3} + \alpha\right) z t^{2\alpha-1} + \frac{2t^{\alpha-1/3}}{(3Q)^{1/3}}\right]\frac{da}{dz} - t^{2\alpha}\, ab = 0. \tag{A2}$$

If $\alpha > 1/2$, the limit $t \to 0$ leads again to a nonphysical solution since $d_z^2 a$ cannot vanish everywhere. Therefore, we conclude that $\alpha = 1/2$ as expected, and Eq. (A2) becomes in the scaling limit

$$\frac{d^2a}{dz^2} + \frac{7z}{6}\frac{da}{dz} = 0, \quad a(-\infty) = 1, \quad a(\infty) = 0, \tag{A3}$$

where

$$z = \left[r - r_f^{\rm ad}(t)\right]/\sqrt{t}, \quad r_f^{\rm ad}(t) = (3Qt)^{1/3}. \tag{A4}$$

The boundary conditions of Eq. (A3) are obtained from $a(r=0,t) = 1$ and $a(r \to \infty, t) = 0$, see Sec. II. Indeed, from Eq. (A4), we have $z \to -\infty$ when $r = 0$ and $t \to 0$, and $z \to \infty$ when $r \to \infty$. Using the derivation performed above, one easily finds that the equation for b is the same as Eq. (A3) with, however, different boundary conditions since $b(r=0,t) = 0$ and $b(r \to \infty, t) = \gamma$:

$$\frac{d^2b}{dz^2} + \frac{7z}{6}\frac{db}{dz} = 0, \quad b(-\infty) = 0, \quad b(\infty) = \gamma. \tag{A5}$$

Before solving the equations for a and b, we first analyze the consequences of this derivation for the maximum of the production rate and its position.

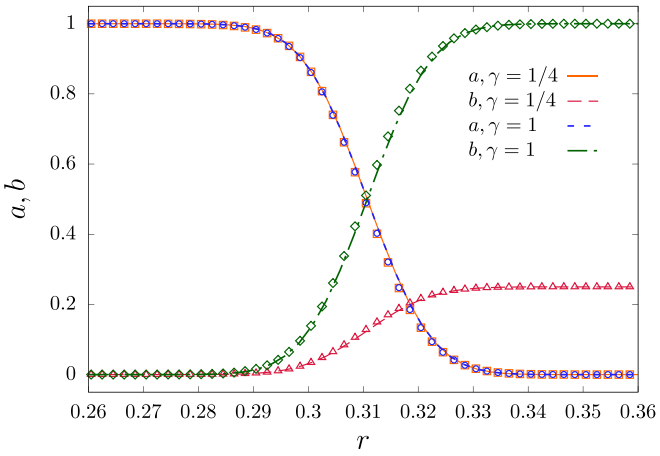

FIG. 10. Early-time concentration profiles a and b for two values of γ and $Q = 100$ at $t = 10^{-4}$. The solid and dashed lines represent the asymptotic solutions (A8), and the symbols represent the solutions obtained by solving numerically Eqs. (3).

1. Production rate

Equations (A3) and (A5) are identical such that if $a(r,t)$ is a solution with the boundary conditions $a(r=0,t)=1$ and $a(r\to\infty,t)=0$, then

$$b(r,t) = \gamma[1 - a(r,t)] \tag{A6}$$

is also a solution with the correct boundary conditions, $b(r\to 0,t)=0$ and $b(r\to\infty,t)=\gamma$. Hence, the early-time production rate $R_E = ab$ reads

$$R_E(r,t) = \gamma a(r,t)[1 - a(r,t)], \tag{A7}$$

whose maximum, obtained from $\partial_r R_E(r,t) = 0$, is located at $r^{\max}(t)$, which is the solution of $a(r^{\max},t) = 1/2$ since a has no extremum at finite value of r. Substituting this value of a into Eq. (A7) leads to Eq. (26). Note that this expression of $R_E^{\max}$ has been obtained without using the explicit expression of a. Therefore, this relation holds at early times in other geometries as can be seen by inspection of Table I. To obtain the radial position of this maximum, we need to use the expression (A3) of a to solve the equation $a(r^{\max},t) = 1/2$. This immediately leads to Eq. (27).

2. Asymptotic solutions for the concentrations

The asymptotic expression of a and b valid at early times are obtained by solving Eqs. (A3) and (A5). Since those equations are first-order differential equation of the derivatives of the concentration profiles, they are readily solved:

$$a(z) = \frac{1}{2}\left[1 - \mathrm{erf}\left(\sqrt{\frac{7}{12}}\, z\right)\right], \tag{A8a}$$

$$b(z) = \gamma[1 - a(z)], \tag{A8b}$$

where z is given by Eq. (A4). Figure 10 shows the concentration profiles of A and B in the early-time regime obtained by solving numerically Eqs. (3), which are well approximated by Eq. (A8). Note that, as γ changes from 1 to 1/4 such that b is modified, the numerical computation shows that a is essentially unchanged confirming that both concentration profiles are uncoupled at early times.

3. Corrections to the front position

Using the asymptotic solutions (A8), we compute the early-time correction to the advective front motion. By definition, the front position r_f is the location where $a = b$. By using Eqs. (A8) together with $a = b$, we get

$$a(z) = \frac{1}{2}\left[1 - \mathrm{erf}\left(\sqrt{\frac{7}{12}}\, z\right)\right] = \frac{\gamma}{1+\gamma}. \tag{A9}$$

This equation is easily solved for z, and, using Eq. (A4), we obtain the early-time evolution of $r_f(t)$ given by Eq. (21). This means that, at early times, the position of the front, r_f, does not coincide precisely with the position $r^{\max}$ of the maximum of production rate located at r_f^{ad}, in contrast to the result obtained at longer times where $r_f = r^{\max}$ [Eq. (16)]. Therefore, in the early-time regime, the production rate evaluated at the front position, R_f, differs in general from the maximum production rate $R_E^{\max}$ computed in Sec. III A [see Eq. (26)]. For completeness, we can derive the early-time expression of R_f. As discussed above, at $r = r_f$ we find $a = b = \gamma/(1+\gamma)$. Hence, the early-time production rate at the front is

$$R_{\mathrm{fE}} = ab = \gamma^2/(1+\gamma)^2. \tag{A10}$$

Comparing Eqs. (A10) and (26), we conclude that, in the early-time regime, the maximum of the production rate is located at the position r_f where $a = b$ only when the initial concentrations of A and B are equal, i.e., for $\gamma = 1$.

4. Reaction front width

We calculate $w_E(t)$ as the width at half-height of $R_E(r,t)$ given by Eq. (A7). By using Eq. (A7) together with Eqs. (A8), and by imposing $R_E(z) = R_E^{\max}/2 = \gamma/8$, we get the two solutions:

$$z_\pm = \pm 2\sqrt{\frac{3}{7}}\,\mathrm{erf}^{-1}(\sqrt{2}/2). \tag{A11}$$

Using the expression (A4) of z, we obtain the two solutions for the radial distances:

$$r_\pm = r_f^{\mathrm{ad}} \pm 2\sqrt{\frac{3}{7}}\mathrm{erf}^{-1}\left(\frac{\sqrt{2}}{2}\right)\sqrt{t}. \tag{A12}$$

Hence, the early-time reaction front width, $w_E = r_+ - r_-$, reads

$$w_E(t) = 4\sqrt{\frac{3}{7}}\mathrm{erf}^{-1}\left(\frac{\sqrt{2}}{2}\right)\sqrt{t} \simeq 1.95\sqrt{t}. \tag{A13}$$

[1] A. N. Kolmogorov, I. G. Petrovsky, and N. S. Piskunov, Moscow Univ. Bull. Math. **1**, 1 (1937).

[2] R. A. Fisher, Ann. Eugen. **7**, 355 (1937).

[3] J. D. Murray, *Mathematical Biology* (Springer Verlag, Berlin, 2003).

[4] S. Kondo and T. Miura, Science **329**, 1616 (2010).

[5] I. Prigogine and G. Nicolis, *Self-Organization in Nonequilibrium Systems* (John Wiley & Sons, New York, 1977).

[6] R. Kapral and K. Showalter (Eds.), *Chemical Waves and Patterns*, Understanding Chemical Reactivity Vol. 10 (Springer Netherlands, Dordrecht, 1995).

[7] V. Volpert and S. Petrovskii, Phys. Life Rev. **6**, 267 (2009).

[8] V. Mendez, S. Fedotov, and W. Horsthemke, *Reaction-Transport Systems: Mesoscopic Foundations, Fronts, and Spatial Instabilities* (Springer-Verlag, Berlin, 2010).

[9] M. C. Cross and P. C. Hohenberg, Rev. Mod. Phys. **65**, 851 (1993).

[10] D. del Castillo-Negrete, B. A. Carreras, and V. Lynch, Physica D **168**, 45 (2002).

[11] B. A. Grzybowski, *Chemistry in Motion: Reaction-Diffusion Systems for Micro- and Nanotechnology* (John Wiley & Sons, Hoboken, NJ, 2009).

[12] P. J. Ortoleva, *Geochemical Self-Organization* (Oxford University Press, Oxford, 1994).

[13] L. Luquot and P. Gouze, Chem. Geol. **265**, 148 (2009).

[14] B. Heidel, C. M. Knobler, R. Hilfer, and R. Bruinsma, Phys. Rev. Lett. **60**, 2492 (1988).

[15] D. Toussaint and F. Wilczek, J. Chem. Phys. **78**, 2642 (1983).

[16] I. Mastromatteo, B. Toth, and J.-P. Bouchaud, Phys. Rev. Lett. **113**, 268701 (2014).

[17] L. Gálfi and Z. Rácz, Phys. Rev. A **38**, 3151 (1988).

[18] Y.-E. L. Koo and R. Kopelman, J. Stat. Phys. **65**, 893 (1991).

[19] S. H. Park, S. Parus, R. Kopelman, and H. Taitelbaum, Phys. Rev. E **64**, 055102(R) (2001).

[20] Z. Jiang and C. Ebner, Phys. Rev. A **42**, 7483 (1990).

[21] Z. Koza, J. Stat. Phys. **85**, 179 (1996).

[22] H. Taitelbaum, S. Havlin, J. E. Kiefer, B. Trus, and G. H. Weiss, J. Stat. Phys. **65**, 873 (1991).

[23] H. Taitelbaum, Y.-E. L. Koo, S. Havlin, R. Kopelman, and G. H. Weiss, Phys. Rev. A **46**, 2151 (1992).

[24] P. M. J. Trevelyan, Phys. Rev. E **80**, 046118 (2009).

[25] F. A. Williams, *Combustion Theory* (CRC Press, Boca Raton, FL, 1994).

[26] C. M. Gramling, C. F. Harvey, and L. C. Meigs, Environ. Sci. Technol. **36**, 2508 (2002).

[27] F. Brau, G. Schuszter, and A. De Wit, Phys. Rev. Lett. **118**, 134101 (2017).

[28] P. M. J. Trevelyan and A. J. Walker, Phys. Rev. E **98**, 032118 (2018).

[29] D. Brockmann and D. Helbing, Science **342**, 1337 (2013).

[30] F. Haudin, J. H. E. Cartwright, F. Brau, and A. De Wit, Proc. Natl. Acad. Sci. USA **111**, 17363 (2014).

[31] Y. Nagatsu, Y. Ishii, Y. Tada, and A. De Wit, Phys. Rev. Lett. **113**, 024502 (2014).

[32] B. Bohner, B. Endrődi, D. Horváth, and Á. Tóth, J. Chem. Phys. **144**, 164504 (2016).

[33] G. Schuszter, F. Brau, and A. De Wit, Environ. Sci. Technol. Lett. **3**, 156 (2016).

[34] B. Bohner, G. Schuszter, O. Berkesi, D. Horváth, and Á. Tóth, Chem. Commun. **50**, 4289 (2014).

[35] B. Bohner, G. Schuszter, D. Horváth, and Á. Tóth, Chem. Phys. Lett. **631–632**, 114 (2015).

[36] V. Sebastian, S. A. Khan, and A. Kulkarni, J. Flow Chem. **7**, 96 (2017).

[37] B. M. Shipilevsky, Phys. Rev. E **70**, 032102 (2004).

[38] B. M. Shipilevsky, Phys. Rev. E **95**, 062137 (2017).

[39] F. W. J. Olver, D. W. Lozier, R. F. Boisvert, and C. W. Clark, editors, *NIST Handbook of Mathematical Functions* (Cambridge University Press, Cambridge, 2010).

[40] A. Baklid *et al.*, in *SPE Annual Technical Conference and Exhibition* (Society of Petroleum Engineers, Richardson, Texas, 1996).

[41] F. Brau and A. De Wit, Influence of rectilinear versus radial advection on the yield of $A + B \rightarrow C$ reaction fronts: A comparison (unpublished).